Вариации оптической и инфракрасной прозрачности атмосферы Земли под действием космических лучей и изменение термодинамических параметров атмосферы

И.В.Кудрявцев

Физико-Технический Институт им А.Ф. Иоффе РАН,
С.- Петербург, Россия

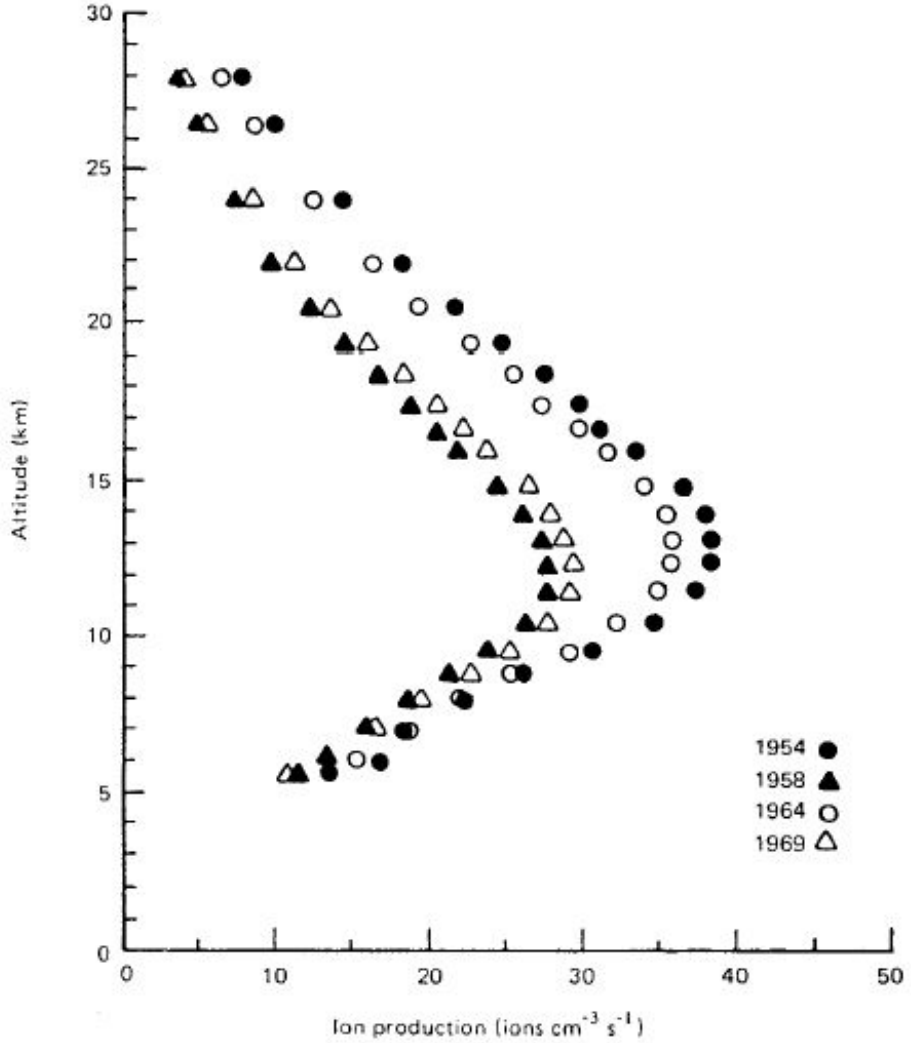

Figure 3. Variability over a solar cycle in the vertical profiles of Ion pair production over Thule, which is situated at a high magnetic latitude (adapted from Neher, 1971). Due to geomagnetic shielding, the levels of ionisation are reduced at lower latitudes, but essential features in the vertical profile are similar.

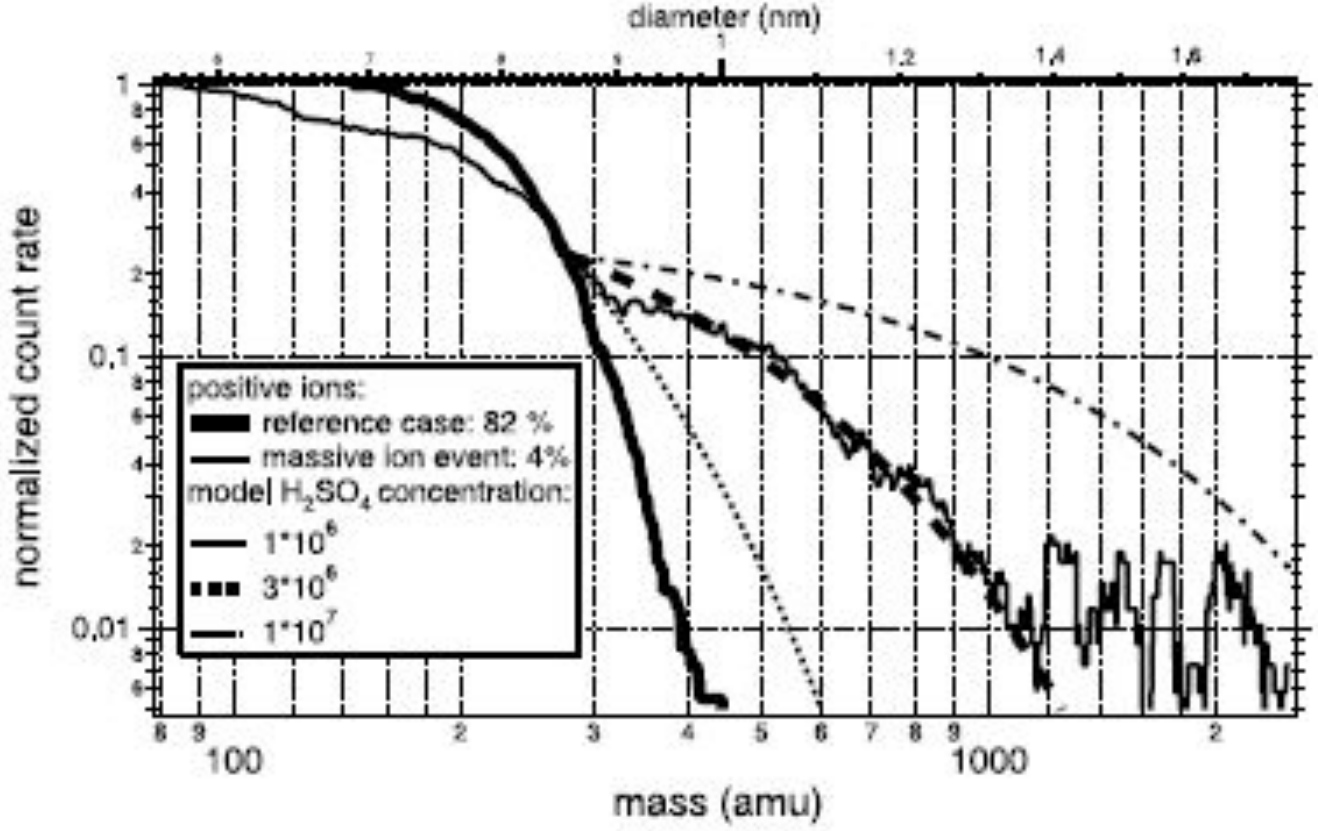

High-Pass-Mode (HPM) mass spectra of positive ions, obtained by mass spectrometric measurements in the upper troposphere and additionally 3 modeled spectra for H_2SO_4 concentrations of $1*10^6$, $3*10^6$ and $1*10^7$ cm^{-3}. Spectrum 1: Reference case, ions up to an m of 400 are present. Spectrum 2: Massive ion event, ions up to a m of 2500 are present (*S. Eichkorn et al,2002)*

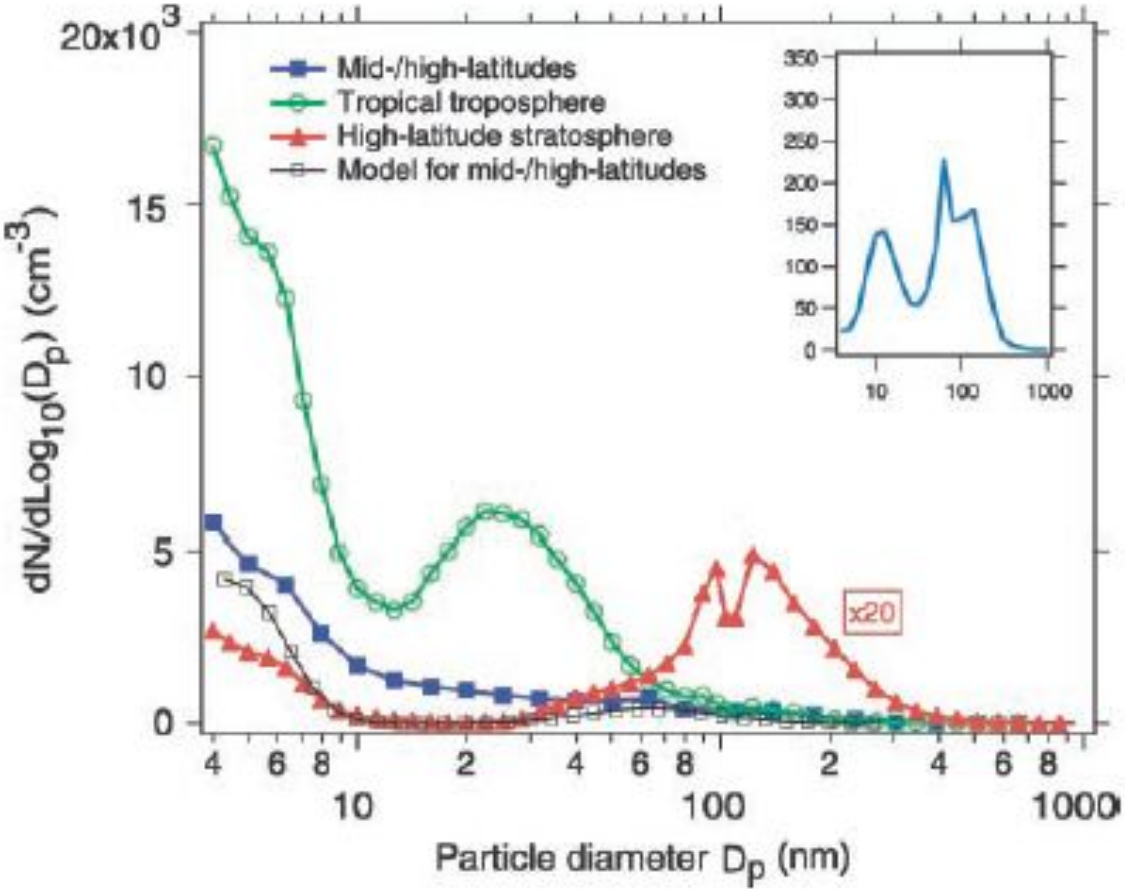

Fig. Mean size distributions for cases satisfying the criteria for recent new particle formation: mid- and high-latitude UT/LS (7 to 13 km), tropical troposphere (7 to 17km) and high-latitude stratosphere (17 to 21km). Results from a simulation of the IIN model after 2-day nucleation evolution are shown for a comparison with the mid- and high-latitude UT/LS case. The model uses _80% of the measured peak noontime *P*H2SO4 and the other average conditions observed for samples showing the feature of new particle formation (table S1). (**Inset**) The average size distribution at the mid- and high latitudes for samples showing no recent particle formation. (*Lee et al, 2003)*

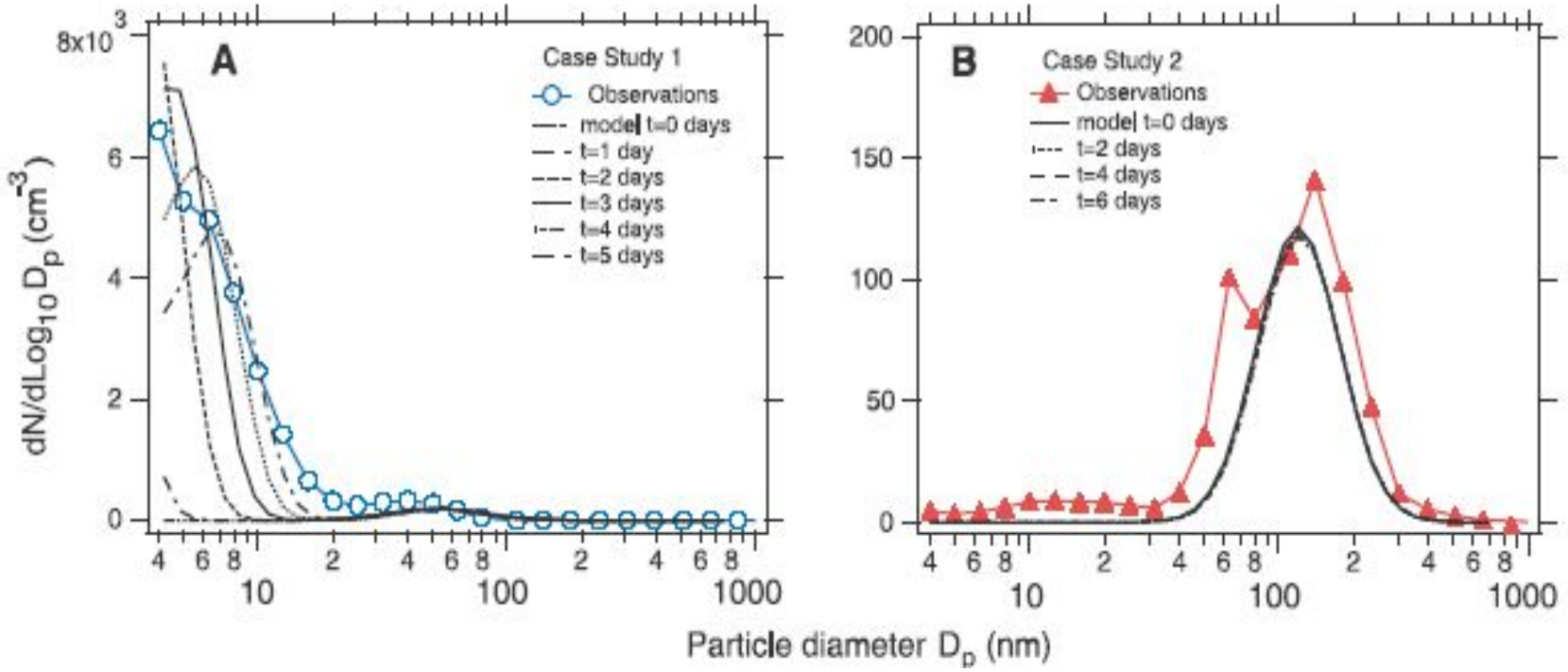

Fig.2. Comparison of measured and simulated particle- size distributions for two cases: high and low ultrafine particle production. (**A**) Particle number-size distributions measured over 18 minutes on 25 January 2000 at 11.2 km, latitudes from 59°N to 60°N, and longitudes from 4°E to 6°E (blue circles). Particle size distributions as a function of time as simulated by the IIN model (black curves). The model uses a peak noontime P_{H2SO4} of 300 cm^{-3} s^{-1}, corresponding to [OH] of two-thirds of the measured value and a fractional sun exposure of 0.25. Other input parameters, including a background particle mode, were as measured in flight (table S1). The $[H_2SO_4]$ derived from the model is ~$1*10^6$ cm^{-3}. (**B**) Particle-size distributions measured over a 12-minute period on 10 December 1999 at 12.5 km, latitudes from 67°N to 70°N, and longitudes from 19°E to 22°E (red triangles). Particle-size distributions as a function of time as simulated by the IIN model, initialized with parameters measured aboard the aircraft (table S1), (black curves).

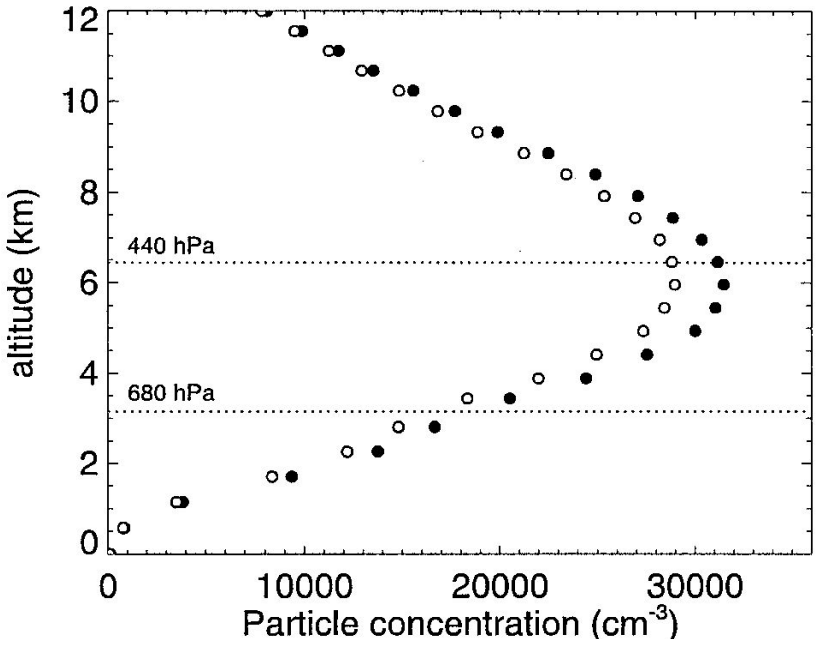

Fig. Concentration of particles of aerosol larger that 3 nm in diameter, formed during 3 hours

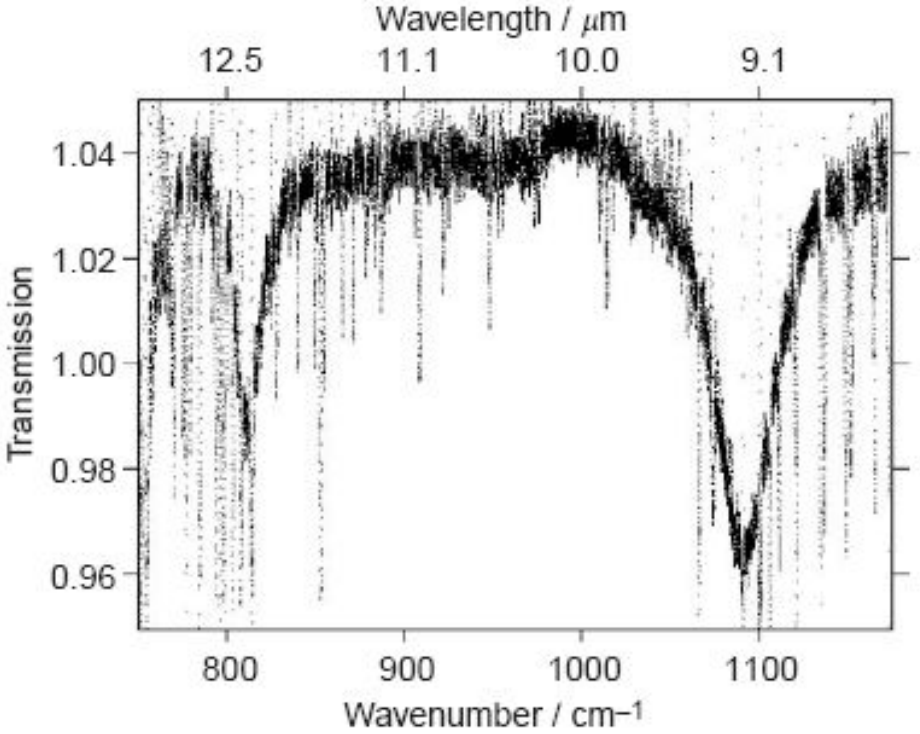

Fig. IR spectrum with enhanced ionisation divided by spectrum from ambient background ionisation, showing areas of enhanced absorption at 12.3 and 9:1 mm (810 and 1095cm^{-1}). The absorption at 13 mm is due to CO_2. Absorption bands, likely to be from molecular cluster-ions can be seen at 12.3 and 9:2 mm (815 and 1090cm^{-1}) (Aplin and McPheat, 2005)

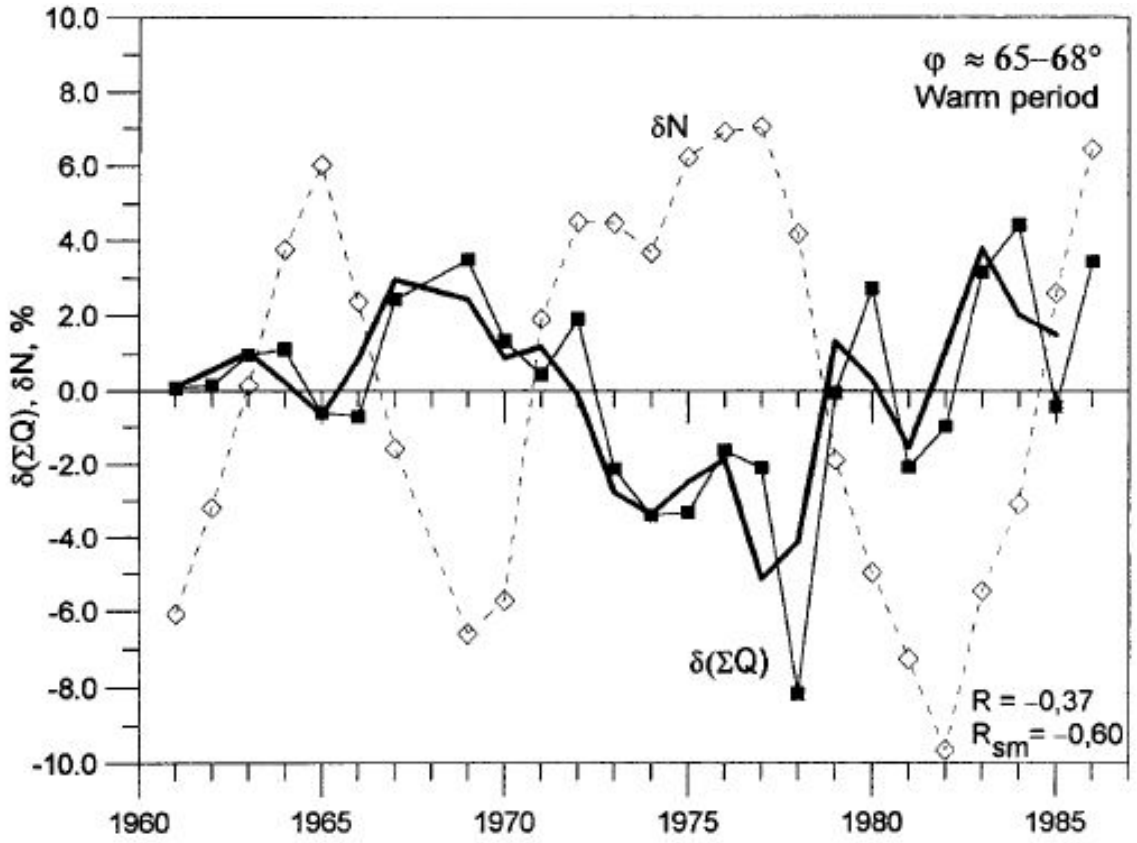

Fig. Long-term variations of the solar radiation input δ(SQ) in the geographic latitudinal belt j165±688 (thin line) and of GCR intensity dN (dashed line); the thick line displays the 2-yr running average of δ(ΣQ) *S.V. Veretenenko*, M.I. Pudovkin,* 1999.

It is possible to separate two steps in the process of generation of NO_3^- ion *(G.A.M. Dreschhoff1, ...,I.V. Koudriavtsev et al, 1999).*
At first step the capture of electron by oxygen and nitrogen molecules and origination of O_3^- takes place

$$e^- + O_2 \rightarrow O^- + O;\ O^- + O_2 + M \rightarrow O_3^- + M\ (M = N_2, O_2)$$
$$e^- + O_3 \rightarrow O_3^-$$
$$e^- + O_3 + O_2 \rightarrow O_3^- + O_2$$

At second step the interaction between ion O_3^- and molecules NO_x takes place. This interaction leads to the origination of the ions NO_3^- and molecules CO_2.

$$O_3^- + CO_2 \rightarrow CO_3^- + O_2;\ CO_3^- + NO_2 \rightarrow NO_3^- + CO_2$$
$$\rightarrow NO_2^- + \ldots;\ NO_2^- + O_3 \rightarrow NO_3^- + \ldots$$

$$O_3^- + NO_2 \longrightarrow NO_3^- + \ldots$$

$$O_3^- + NO \rightarrow NO_2^- + \ldots;\ NO_2^- + O_3 \rightarrow NO_3^- + \ldots$$

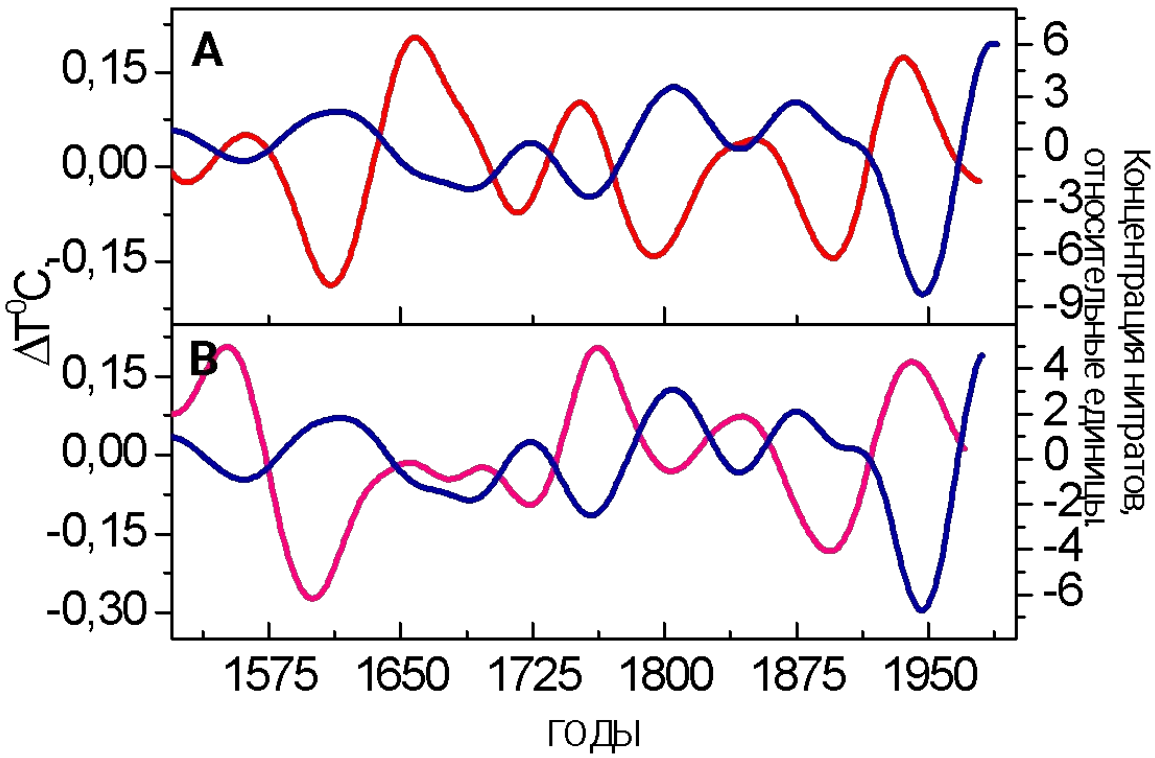

Рис. Временные серии вэйвлетно-фильтрованные в полосе 55-147 лет (использован базис МНАТ).

А– кривая 1 – H1, кривая 2 - июльская температура в континентальной части северной Фенноскандии [Lindholm and Eronen, 2000]; В – кривая 1 – H1, кривая 2 - средняя температура сезона вегетации в приморской части северной Фенноскандии [Briffa et al., 1992];

(Огурцов,2002)

ОСНОВНЫЕ УРАВНЕНИЯ

$$\frac{dW}{dz} = \alpha_1 \rho(1+\delta_1)W \quad ; \quad \frac{dA}{dz} = \alpha_2 \rho(1+\delta_2)(A - fE) \quad ; \quad \frac{dB}{dz} = \alpha_2 \rho(1+\delta_2)(fE - B)$$

$$dQ = (\alpha_1 \rho(1+\delta_1)W + \alpha_2 \rho(1+\delta_2)A + \alpha_2 \rho(1+\delta_2)B - 2\alpha_2 \rho(1+\delta_2)fE + (\frac{d}{dz}\lambda\frac{dT}{dz}))dz$$

где ***W-*** поток солнечного коротковолнового (видимого) излучения;
A. B- потоки инфракрасного излучения, распространяющиеся вниз и вверх; α_1 , α_2 - коэффициенты поглощения видимого и инфракрасного излучения в атмосфере, без учета дополнительного поглощения, вызванного влиянием КЛ ; δ_1, δ_2 - описывает дополнительное поглощение видимого и инфракрасного излучения, вызванное влиянием КЛ; $E=\sigma T^4$, σ - постоянная Стефана-Больцмана; T – температура воздуха; коэффициент $f<1$ показывает, на сколько длинноволновое излучение атмосферы меньше чем излучение абсолютно черного тела.

$$\delta_1 = \frac{\delta_{10}}{\sqrt{2\pi}\sigma_1} exp(-(\tau_v - \tau_{vo})^2 / (2{\sigma_1}^2))$$

$$\delta_2 = \frac{\delta_{20}}{\sqrt{2\pi}\sigma_2} exp(-(\tau - \tau_o)^2 / (2\sigma^2))$$

$$\tau_v = \int_z^\infty \alpha_1 \rho(h)dh$$

$$\tau(z) = \int_z^\infty \alpha_2 \rho(h)dh$$

$\sigma_1 = \beta\sigma$, ; $\tau_{v0} = \beta\tau_0$; , т.е. $\tau_v = \beta\tau$; $\tau(0) = 3.78$, $\beta = \alpha_1/\alpha_2 = 0.2$

1) Долговременные вариации прозрачности и распределения температуры в атмосфере.
dQ =0

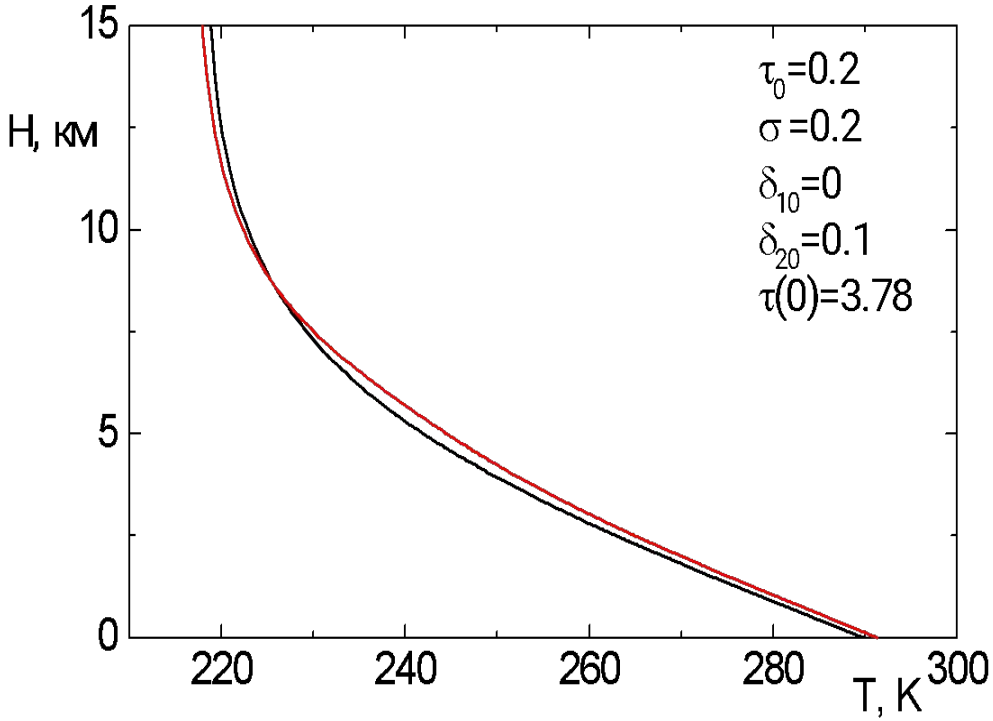

Рис. Распределение температуры в атмосфере

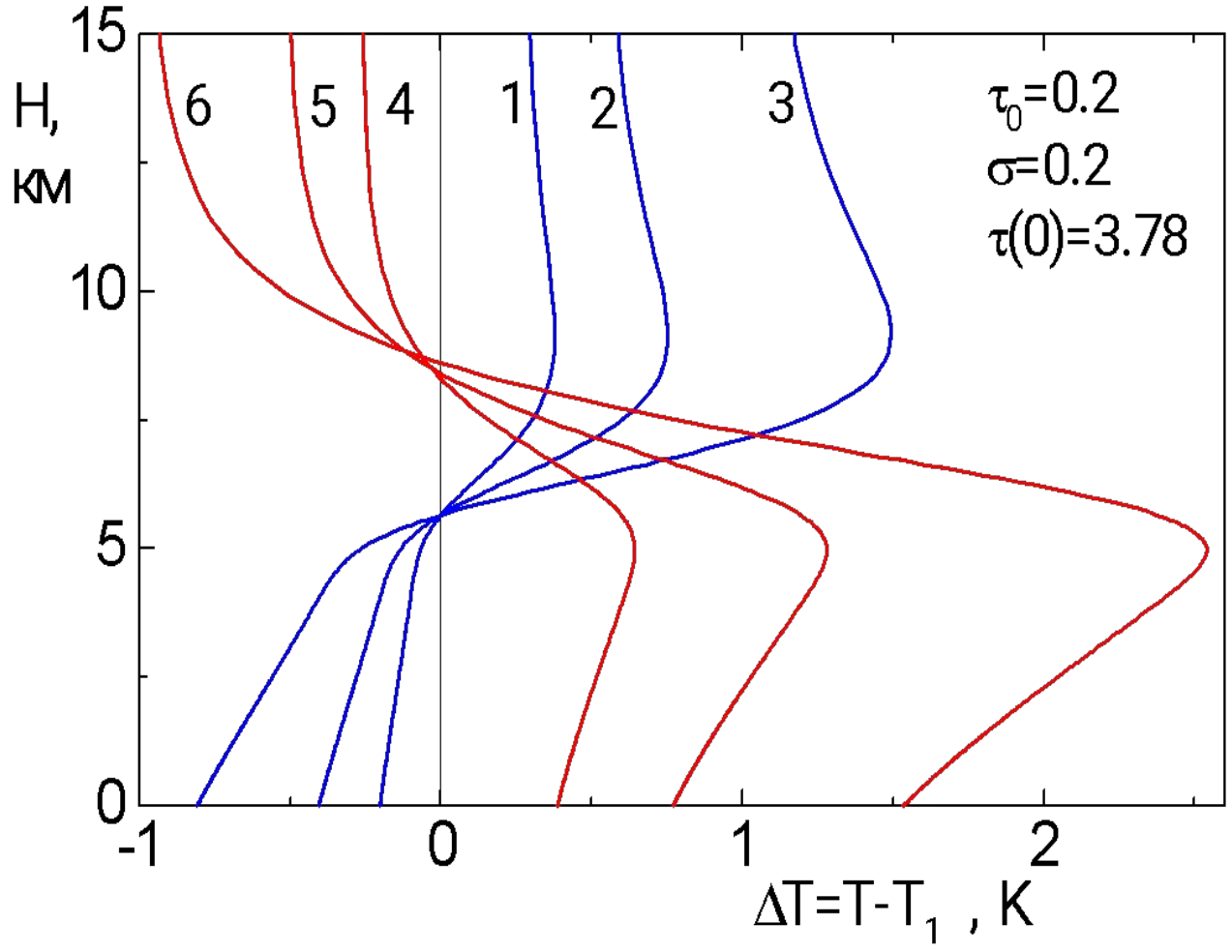

Изменение температуры $\Delta T=T-T_1$ для различных значений поглощающего слоя:
1 -δ_1 =0,005; δ_2=0; 2 -δ_1 =0,01; δ_2=0; 3 -δ_1 =0,02; δ_2=0;
4 -δ_1 =0; δ_2=0,025; 5 -δ_1 =0; δ_2=0,05; 6 -δ_1 =0; δ_2=0,1

Кратковременные вариации прозрачности и распределения температуры в атмосфере

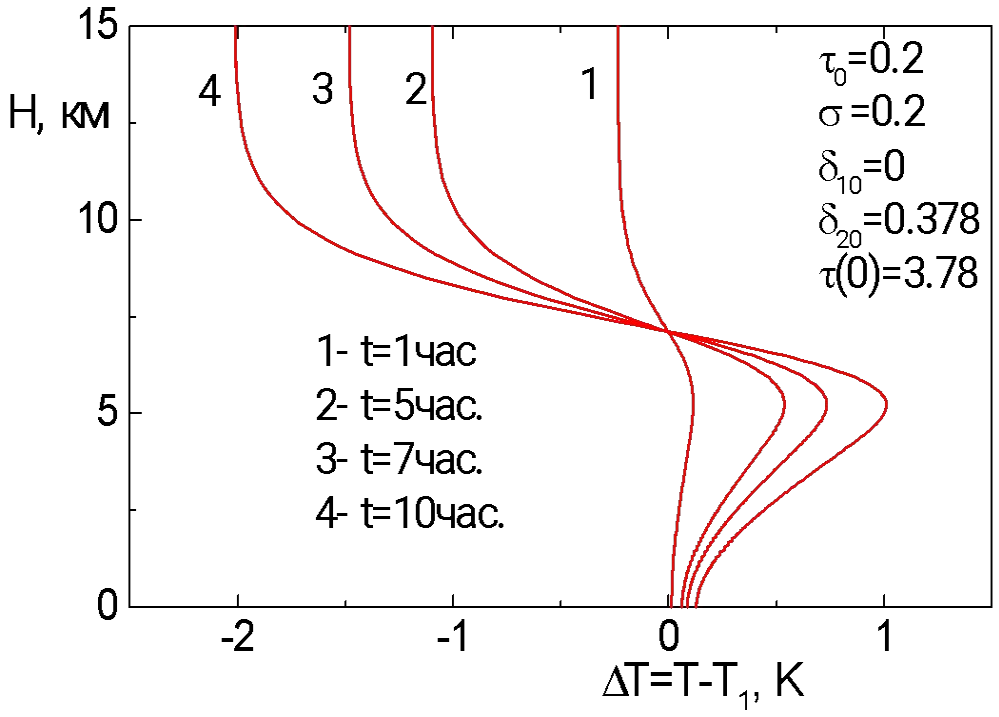

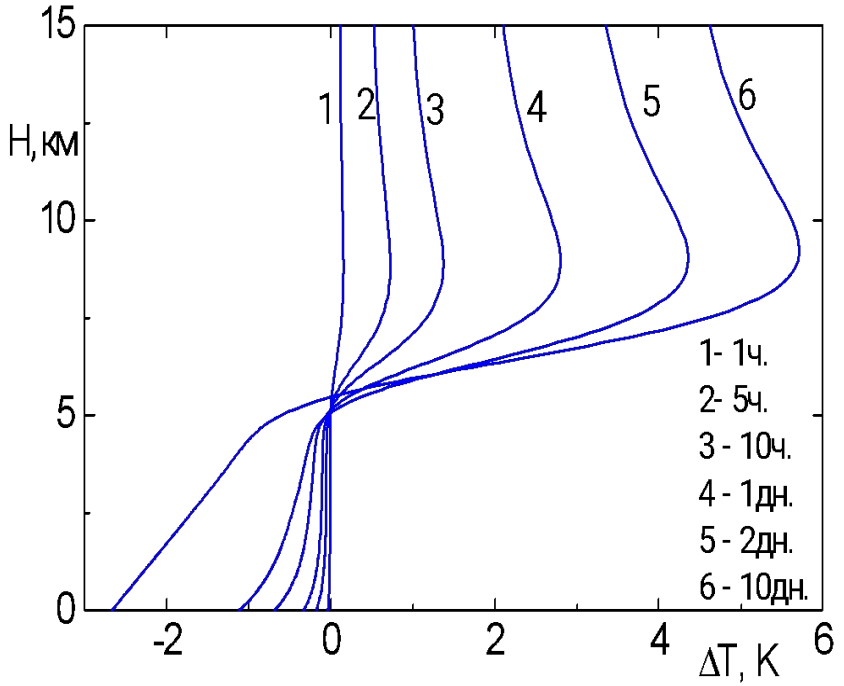

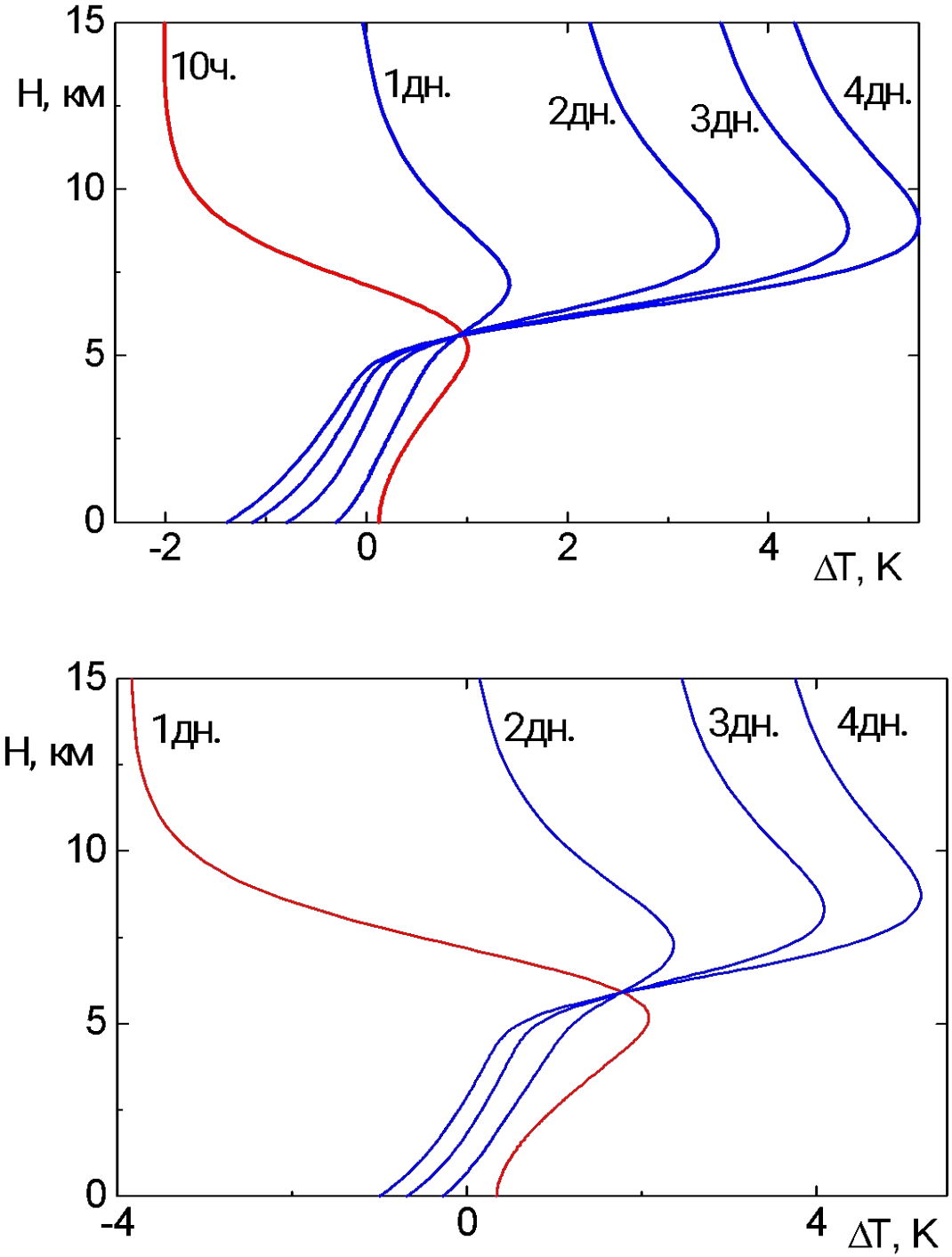
15
10
5
0
H, км
10ч.
1дн.
2дн.
3дн.
4дн.
-2
0
2
4
ΔT, K
15
10
5
0
H, км
1дн.
2дн.
3дн.
4дн.
-4
0
4
ΔT, K

Вариации атмосферного давления

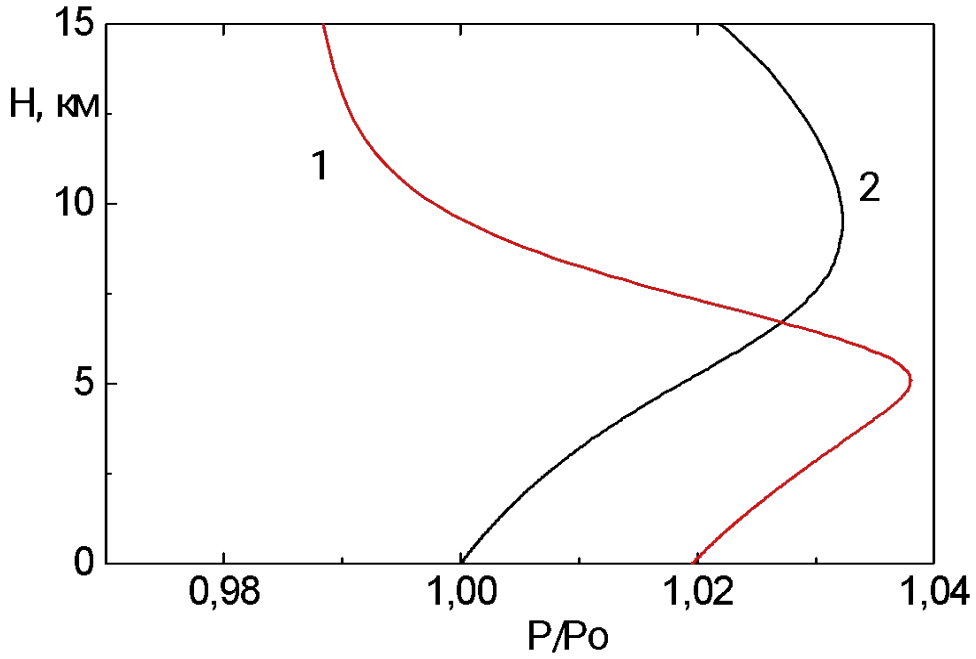

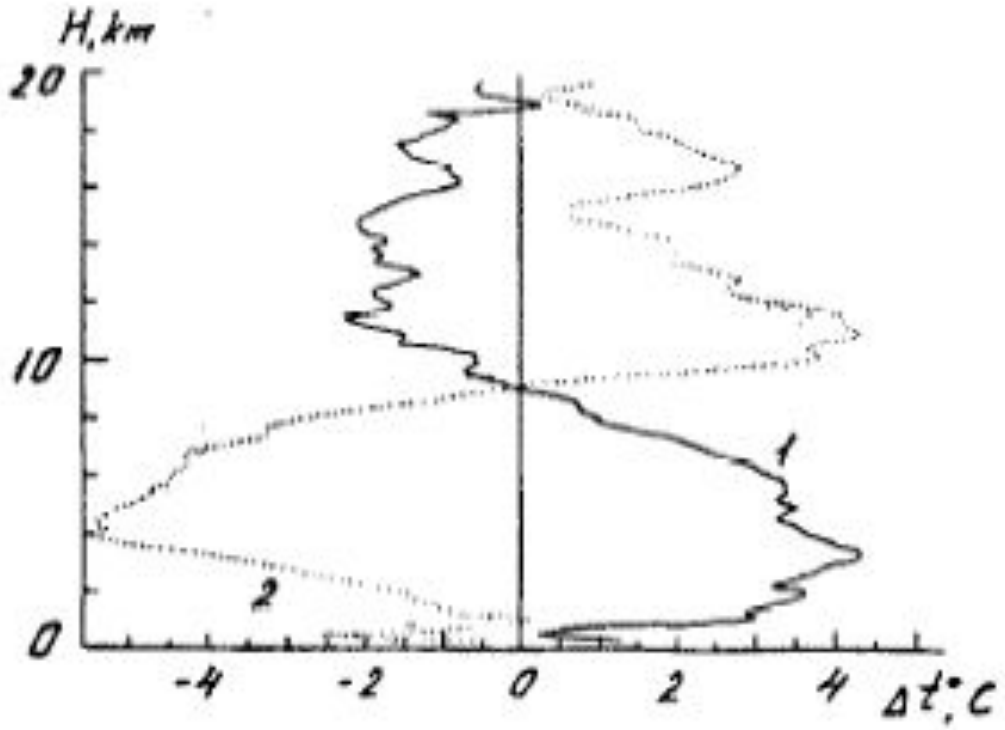

Variations of the mean temperature profiles for the anticyclonic conditions before the SCR burst:
1 - on the key day *(t=O):* 2 - on the third day *(t=+3). (M. I. Pudovkin et al, 1996)*.

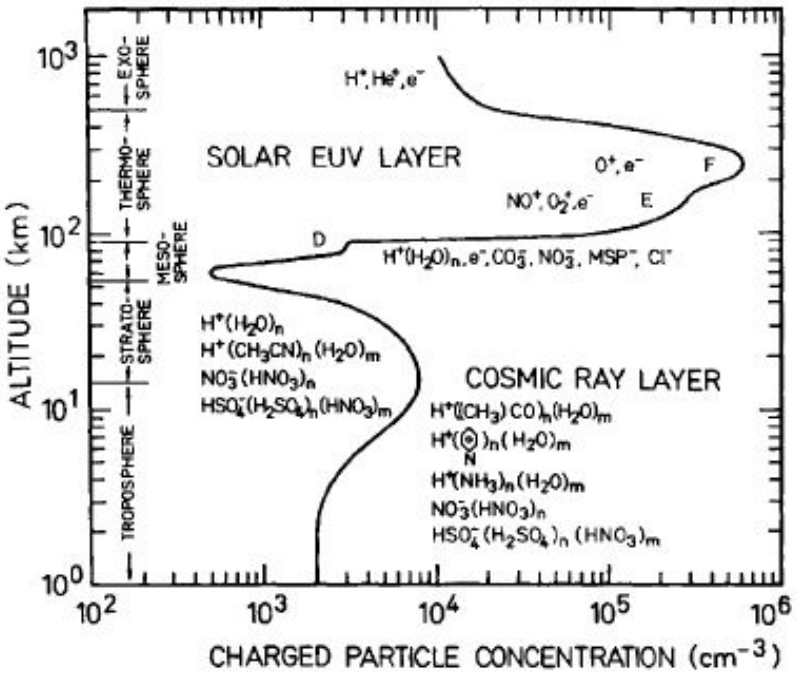

Figure 8. Vertical Profile of ionisation density in the atmosphere. Included are the major ion species at various altitudes (adapted from Viggiano and Arnold, 1995).

$$dQ = \frac{C_v \rho_в dT}{dt} dz$$

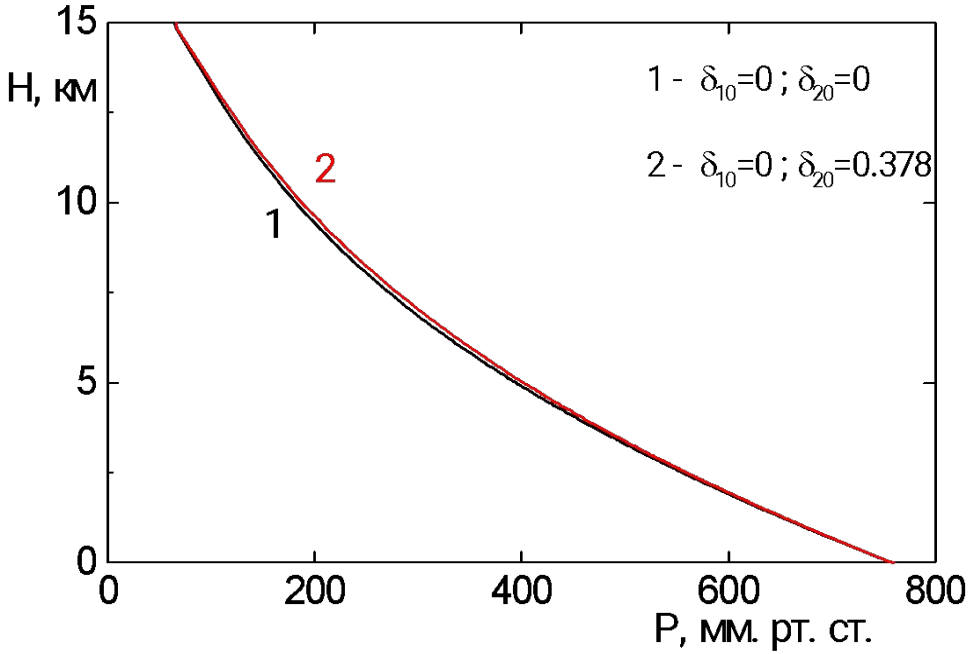
15
10
5
0
H, км
0
200
400
600
800
P, мм. рт. ст.
1 - δ10=0 ; δ20=0
2 - δ10=0 ; δ20=0.378
1
2